J. Cell. Mol. Med. Vol 12, No 6B, 2008 pp. 2609-2621

The induction of bone formation by *smart* biphasic hydroxyapatite tricalcium phosphate biomimetic matrices in the non-human primate *Papio ursinus*

U. Ripamonti [a, *], P. W. Richter [b], R. W. N. Nilen [b], L. Renton [a]

[a] *Bone Research Unit, Medical Research Council/ University of the Witwatersrand, Johannesburg, South Africa*
[b] *Materials Science & Manufacturing Technology, Council for Scientific and Industrial Research, Pretoria, South Africa*

Received: November 1, 2007; Accepted: March 13, 2008

Abstract

Long-term studies in the non-human primate Chacma baboon *Papio ursinus* were set to investigate the induction of bone formation by biphasic hydroxyapatite/β-tricalcium phosphate (HA/β-TCP) biomimetic matrices. HA/β-TCP biomimetic matrices in a pre-sinter ratio (wt%) of 40/60 and 20/80, respectively, were sintered and implanted in the *rectus abdominis* and in calvarial defects of four adult baboons. The post-sinter phase content ratios were 19/81 and 4/96, respectively. Morphological analyses on day 90 and 365 showed significant induction of bone formation within concavities of the biomimetic matrices with substantial bone formation by induction and resorption/dissolution of the implanted matrices. One year after implantation in calvarial defects, 4/96 biphasic biomimetic constructs showed prominent induction of bone formation with significant dissolution of the implanted scaffolds. The implanted *smart* biomimetic matrices induce *de novo* bone formation even in the absence of exogenously applied osteogenic proteins of the transforming growth factor-β (TGF-β) superfamily. The induction of bone formation biomimetizes the remodelling cycle of the cortico-cancellous bone of primates whereby resorption lacunae, pits and concavities cut by osteoclastogenesis are regulators of bone formation by induction. The concavities assembled in HA/β-TCP biomimetic bioceramics are endowed with multifunctional pleiotropic self-assembly capacities initiating and promoting angiogenesis and bone formation by induction. Resident mesenchymal cells differentiate into osteoblastic cell lines expressing, secreting and embedding osteogenic soluble molecular signals of the TGF-β superfamily within the concavities of the biomimetic matrices initiating bone formation as a secondary response.

Keywords: biphasic hydroxyapatite β-tricalcium phosphate bioceramics • biomimetism • osteogenic proteins of the TGF-β superfamily • bone induction

Introduction

Regenerative medicine and tissue engineering of bone start by constructing scaffolds of biomimetic matrices that mimic the supramolecular assembly of the extracellular matrix of bone [1, 2]. Biomimetic matrices control the expression of the osteogenic soluble molecular signals of the transforming growth factor-β (TGF-β) superfamily, proteins initiating *de novo* bone formation by induction [1, 2]. In clinical contexts, the induction of bone formation with *restitutio ad integrum* of missing skeletal parts has been controversial and is still a rather elusive and difficult goal often unattainable in severe acute and chronic human conditions [3, 4]. This is despite the use of high doses of recombinant human bone morphogenetic and osteogenic proteins (hBMPs/OPs) [3–11]. After exciting and rewarding years of research in regenerative medicine, tissue engineering of bone, and pre-clinical experiments including results in non-human primates [1, 2, 12–14], skeletal reconstructionists, tissue engineers and molecular biologists alike were led to believe that single applications of selected single recombinant hBMPs/OPs would restore skeletal deficiencies in human patients adding a new and effective molecular tool for regenerative medicine and bone tissue engineering in clinical contexts [1, 2, 12–16]. The induction of bone formation by doses of hBMPs/OPs has been often punctuated by the lack of total and/or convincing regeneration

*Correspondence to: Ugo RIPAMONTI, M.D., Ph.D.,
Director, Bone Research Unit, Medical Research Council/University of the Witwatersrand, Medical School, 7 York Road, 2193 Parktown, Johannesburg, South Africa.
Tel.: +27 11 717 2144
Fax: +27 11 717 2300
E-mail: ugo.ripamonti@wits.ac.za

doi: 10.1111/j.1582-4934.2008.00312.x

of the missing part of bone so often needed in unfavourable clinical conditions [3–11].

This paper proposes tissue engineering of bone with complete *restitutio ad integrum* of non-healing calvarial defects of adult non-human primates *Papio ursinus* by biphasic biomimetic *smart* hydroxyapatite (HA) β-tricalcium phosphate (β-TCP) matrices that *per se* are endowed with the striking prerogative of initiating *de novo* bone formation by induction without exogenously applied osteogenic proteins of TGF-β superfamily [2, 14–16]. Importantly, post-sinter biphasic HA/β-TCPof 4/96 (wt%) biomimetic calvarial constructs were almost completely resorbed by invocation of a generated downstream cascade of cellular and molecular events leading to the generation of resorption lacunae carved by osteoclast- and/or macrophage like-cells that ultimately initiated the spontaneous induction of bone formation. The geometric concavity of the induced resorption lacunae set into motion the biomimetic induction of bone formation ultimately replacing the implanted biomimetic matrices.

The extent of resorption and/or dissolution of biphasic calcium phosphate bioceramics has been essentially investigated in rodent, lagomorph and canine models, and very limited studies have been reported using non-human primate species [17, 18]. After implantation of coral-derived hydroxyapatites with different ratios of calcium phosphate to calcium carbonate with or without highly purified naturally-derived BMPs/OPs [2], results showed limited if any biomatrix resorption over time in heterotopic *rectus abdominis* sites [17]. In orthotopic sites, both control and BMPs/OPs-treated specimens showed variable but often extensive resorption and dissolution of the implanted porous substrata [18]. Importantly, however, the implanted porous scaffold was substituted not by bone but by a dense fibrovascular tissue enveloping islands of newly formed bone in calvarial defects of adult baboons [18]. Biphasic bioceramic constructs with 40wt% β-TCP content implanted in calvarial defects of adult baboons showed the lack of biomatrix resorption as evaluated histomorphometrically on day 30 and 90 after implantation [19].

The basic tissue engineering paradigm is tissue and organ development engineered by combinatorial molecular protocols. Soluble molecular signals are combined and reconstituted with insoluble signals or substrata that act as three-dimensional scaffolds for the initiation of *de novo* tissue induction and morphogenesis [1, 2, 12–16]. This study proposes a biphasic HA/β-TCP biomimetic construct capable not only to initiate the spontaneous induction of bone formation but also to resorb resulting in the induction of bone formation replacing *in toto* the implanted biomimetic matrices with *restitutio ad integrum* of the calvarial defects. We wished thus to change the paradigm by deploying *smart* biomimetic constructs that in their own right not only induce the initiation of bone formation without the addition of exogenously applied osteogenic proteins of the TGF-β superfamily [2, 20] but that also significantly resorb resulting in the induction of bone formation replacing the porous spaces and the implanted biomimetic scaffold.

Long-term studies in the non-human primate *Papio ursinus* were set to study the induction of bone formation by biphasic HA/β-TCP biomimetic constructs with post-sinter phase content ratios (wt%) of 19/81 and 4/96, respectively. The most striking observation was that the induction of resorption lacunae and concavities set into motion the intrinsic induction of bone formation replacing the implanted biomimetic matrices in a *continuum* of resorption/dissolution and induction of bone formation. Morphological and histomorphometric analyses of tissue specimens harvested 365 days after heterotopic and orthotopic implantation showed significant induction of bone formation with prominent resorption/dissolution of the implanted biomimetic matrices with *restitutio ad integrum* of the calvarial defects.

Materials and methods

Hydroxyapatite powder preparation

Hydroxyapatite (HA) was synthesized by solid state reaction [21–23] between β-TCP (Merck No. 2143) and Ca $(OH)_2$ (Saarchem Univar No. 1525220). The starting powders were combined in appropriate quantities for a Ca/P molar ratio of 1.67 (the ratio for stochiometric HA), mixed in deionized water performed with a high speed Silverson homogenizer (Silverson Machines, Inc., Longmeadow, MA, USA) for 20 min. The resulting slurry was gelled to prevent powder separation during drying at 100°C for 15 hrs. The dried slurry was reacted at 1000°C for 18 hrs to produce HA by: $3\beta\text{-}Ca_3(PO_4)_2 + Ca(OH)_2 \rightarrow Ca_{10}(PO_4)_6(OH)_2$ [24]. The resulting HA was ball-milled for 24 hrs in a polyurethane-lined ball mill using zirconia milling media, to achieve a median grain size of approximately 0.6 μm. The phase purity was confirmed by X-ray diffraction (XRD, Philips, Cu-Kα, 45kV, 40 mA), and Fourier transform infrared spectroscopy (FTIR Thermo Nicolet, 400–4000 cm^{-1} range, 4 cm^{-1} resolution).

Biphasic calcium phosphate sample preparation

HA and β-TCP (Fluka No. 21218) powders were combined to form batches with pre-sinter HA/β-TCP content ratios (wt%) of 40/60 and 20/80, respectively. Batches were mixed in deionized water slurries performed with a high speed Silverson homogenizer, and then dried for 15 hrs at 100°C. A 10wt% binder phase of PEG 400 diluted in ethanol (1 part PEG 400 to 4 parts ethanol) was hand mixed into the powder in flowing air on a magnetic stirrer to maintain a homogenous binder distribution during ethanol evaporation and dried overnight at 60°C. The powder agglomerates were sieved below 200 μm and green body discs uniaxially pressed at 20 MPa at room temperature. The discs for heterotopic implantation were 20 mm in diameter and 3 mm thickness with 25 hemispherical indentations of 2 mm diameter on one planar surface only. Additional discs of single phase HA with a Ca/P molar ratio of 1.67 were prepared *via* a solid state reaction [19] and used for heterotopic implantation only. Macroporous samples were pressed from powders containing stearic acid spheres of between 0.7 and 1 mm in diameter to construct porous discs 25 mm in diameter and 4 mm thick for orthotopic calvarial implantation. Samples were sintered pressureless in air for 1 hr at 1020°C, with the furnace cycle up and down rates fixed at 100°C per hour after debinding of the fugitive phase [25].

Sample characterization

All samples were analysed using XRD (Philips, Cu-Kα, 45 kV, 40 mA), FTIR (Thermo Nicolet, 400–4000 cm^{-1} range, 4 cm^{-1} resolution) and scanning

electron microscopy (LEO 1525 field emission FE-SEM), both before and after sintering.

For the XRD measurements, a 2θ scan range of 4–70° with 0.02° steps and 10 sec. counts per step was used. The X'Pert HighScore® analysis package was used to quantify the HA: β-TCP phase content ratio using the Powder Diffraction File® database (PDF) reference patterns 74-0566 (HA) and 70-2065 (β-TCP) [26].

Primate models for tissue induction

Four clinically healthy adult Chacma baboons *Papio ursinus*, with a mean weight of 14.7 ± 0.67 kg, were selected from the primate colony of the University of the Witwatersrand, Johannesburg. Criteria for selection, housing conditions and diet were as described [14, 27]. Research protocols were approved by the Animal Ethics Screening Committee of the university, and conducted according to the *Guidelines for the Care and Use of Experimental Animals* prepared by the University and in compliance with the *National Code for Animal Use in Research, Education and Diagnosis in South Africa* [28].

The heterotopic *rectus abdominis* and orthotopic calvarial models of tissue induction and morphogenesis by osteoinductive biomimetic matrices have been described in details [2, 14–20, 27]. A total of 12 solid discs with concavities only on one planar surface were implanted bilaterally in 12 ventral intramuscular pouches created by sharp and blunt dissection in the *rectus abdominis* muscle of each animal. Phase pure solid HA, biphasic pre-sinter HA/β-TCP content ratios (wt%) of 40/60 and 20/80 biomimetic matrices were implanted in quadruplicate two samples with the concavities facing ventrally and two samples with concavities facing dorsally to evaluate the extent of bone induction as directed by the site of implantation within the *rectus abdominis* muscle (Fig. 1A).

After heterotopic implantation, the calvariae were exposed and, on each side of the calvarium, two full-thickness defects, 25 mm in diameter, each separated by 2.5–3 cm of intervening calvarial bone, were created with a craniotome under saline irrigation [2, 14–20]. A contra lateral Latin Square Block design was used to allocate the position of the sintered HA/β-TCP biphasic biomimetic matrices, two specimens per animal, for a total of 8 pre-sinter content ratios (wt%) of 40/60 and 8 pre-sinter content ratios 20/80 HA/TCP biphasic biomimetic matrices (Fig. 1B).

Tissue harvest, histology and histomorphometry

Anaesthetized animals were killed with an intravenous overdose of sodium pentobarbitone on day 90 and 365, two animals per observation period. Anaesthetized animals were subjected to bilateral carotid perfusion and harvest of specimens with surrounding calvaria as described [14–20]. Specimen blocks were cut along the sagittal one-third of the implanted defects, further fixed in 10% neutral buffered formalin, decalcified electrolytically in a Sakura TDE™30 decalcifying unit (Sakura, Fintek, USA) and processed for paraffin wax embedding. Sections, cut at 4 μm, were stained with heamatoxylin-eosin or a modified Goldner's modified trichrome [2, 14–20].

Heterotopic tissue sections of single phase HA, and biphasic HA/ β-TCP biomimetic constructs, were analysed to quantitate the percentage of newly formed bone by induction within the concavities of the substrata in relation to the total area of the inducing concavity. The cross-sectional area (in %) of induced bone in the concavities of the implanted biomimetic matrices was measured using a computerized image analysis system (analySIS™ Soft Imaging System, Münster, Germany) attached to a capturing video-camera (WV-CP 410/G Panasonic, Tokyo, Japan) [2, 19]. The measurements were used to calculate a ratio of area of bone/area of concavity and expressed as a percentage and are presented in Table 1.

Orthotopic specimen blocks were cut along the sagittal third of the implanted discs, further fixed in 10% neutral buffered formaldehyde, and electrolytically decalcified as described above. Serial sections 4-μm thick were mounted after recording the position of the anterior and posterior interfaces of the defects with their corresponding calvarial margins. Sections were stained with a modified Goldner's trichrome and examined with a Provis AX70 research microscope (Olympus Optical Co., Japan). A calibrated Zeiss Integration Platte II (Oberkochem, Germany) with 100 lattice points was used to calculate, by the point counting technique [29], the fractional volume (in %) of each of the following histological components: newly formed bone, fibrovascular tissue (including marrow) and the HA/β-TCP substrata. Calvarial sections were analysed at 40X superimposing the Zeiss graticule over five sources selected for histomorphometry and defined as follows: two anterior and posterior interfacial regions (AIF and PIF), two anterior and posterior internal regions (AIN and PIN) and a central region (CEN) [2, 14–19]. Each source represented a field of 7.84 mm^2. Morphometry was performed on two sections per implant, analysing 39.2 mm^2 per section for a total of 32 sections and data are presented in Table 3.

Results

HA synthesis by solid state reaction

XRD analysis of the pure HA synthesized by solid state reaction revealed single phase crystalline HA, with all peaks identified by PDF® pattern 74-0566, with a 97% degree of crystalline, as determined following the method of Landi *et al.* [30]. FTIR spectroscopy revealed the standard HA infrared absorption spectrum with the OH^- stretching mode peak at 3571 cm^{-1}, and the characteristic peaks and bands between 500 and 1150 cm^{-1} assigned to PO_4^{3-} [22, 31, 32].

Macro- and microstructure of sintered biphasic bioceramics

SEM analysis of the sintered biphasic HA/β-TCP bioceramics confirmed the presence of 0.7-1 mm diameter inter-connected macropores, as well as a highly microporous (pores less than 1 μm) biphasic microstructure. SEM micrographs are presented in Fig. 2. The highly microporous nature of the sintered materials (42% open porosity for the solid heterotopic samples and 68% for the macroporous samples) endows the material with an enhanced surface area, and correspondingly, a high degree of bioactivity [33, 34].

Phase content quantification post-sinter

The post-sinter HA/β-TCP phase content ratios of the biphasic bioceramic constructs were determined using the semi-quantitative XRD-based Chung method [26] (*via* the X'Pert HighScore® analysis package). The measurements revealed a decrease in HA intensity

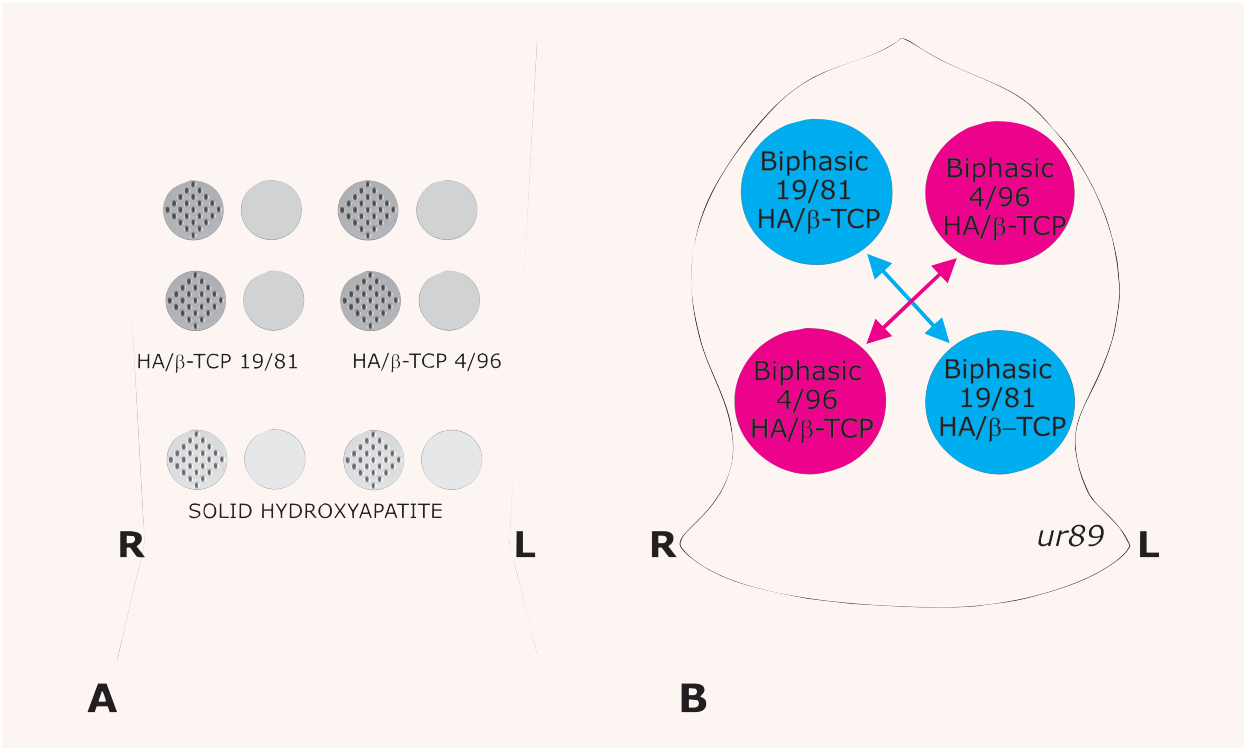

Fig. 1 Heterotopic *rectus abdominis* and orthotopic calvarial models in 4 adult Chacma baboons *Papio ursinus* for bone induction and morphogenesis by sintered biphasic hydroxyapatite (HA) tricalcium phosphate (TCP) with post-sinter content ratios of 19/81 and 4/96, respectively, implanted in both heterotopic *rectus abdominis* and orthotopic calvarial sites. (**A**) Heterotopic intramuscular model and implantation design in the *rectus abdominis* muscle. HA/TCP 19/81, HA/TCP 4/96 and solid hydroxyapatite discs of 20 mm in diameter, 3 mm thickness with 25 hemispherical indentations on one planar surface only were implanted in quadruplicate two samples with the concavities facing ventrally and two samples with concavities facing dorsally to evaluate the extent of bone induction as directed by the site of implantation within the *rectus abdominis* muscle. (**B**) The calvarial Latin block design resulted in the contra lateral implantation of macroporous discs of either post-sinter 19/81 HA/TCP and 4/96 HA/TCP biphasic biomimetic matrices, two macroporous implants per animal for a total of 8 19/81 and 8 4/96 HA/TCP biphasic macroporous discs.

Table 1 Cross-sectional areas (%) of induced bone within concavities of post-sinter 19/81, 4/96 biphasic hydroxyapatite (HA)/ β-tricalcium phosphate (β-TCP) and solid hydroxyapatite (HA) discs implanted in the *rectus abdominis* muscle of four baboons and harvested 90 and 365 days after implantation

Time	Biomimetic matrices	% bone within concavity	Concavities facing *rectus abdominis*	Concavities facing peritoneal fascia
90	19/81 HA/β-TCP	33	32	32
	4/96 HA/β-TCP	28	34	27
	Solid HA	No bone*	-	-
365	19/81 HA/β-TCP	53	44	55
	4/96 HA/β-TCP	45	40	52
	Solid HA	28	24	32

Newly induced bone within the concavities of the biomimetic matrices is expressed as a percentage of the concavity surface area as described in 'Materials and methods'. Volume fractions (%) of newly formed bone within inducing concavities represent values of 5–8 specimens per treatment modality. * Only one of the solid HA samples showed minor bone formation.

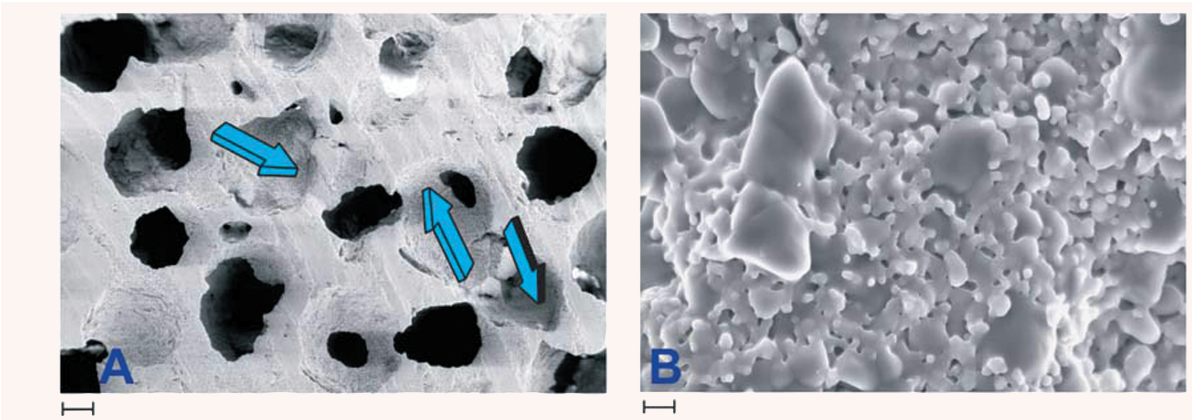

Fig. 2 Scanning electron microphotographs of a specimen of hydroxyapatite/tricalcium phosphate 19/81. (**A**) Blue arrows show repetitive sequences of concavities with defined radii of curvature and diameters in macroporous specimens for orthotopic calvarial implantation. (**B**) Microstructure of the 19/81 biomimetic biphasic constructs. Larger grains are β-tricalcium phosphate, the smaller grains hydroxyapatite. Scale bar in A is 200 μm, in B 1μm

relative to the known pre-sinter HA contents, with an associated increase in β-TCP intensity (Table 2). No crystalline phases other than HA and β-TCP were identified in the sintered samples, so the results suggest the thermal decomposition of some of the HA to β-TCP during sintering. The results presented in Table 2 highlight the significant extent to which the HA phase thermally decomposes to β-TCP during high temperature sintering, which, of course, will significantly affect the overall resorption rate of the materials *in vivo* [24, 25]. Implanted biphasic HA/β-TCP constructs should thus be considered to have β-TCP contents of 81 and 96 wt%, respectively (balance HA), hereafter referred to as 19/81 HA/β-TCP and 4/96 HA/β-TCP biphasic constructs (Table 2).

Table 2 Hydroxyapatite (HA)/β-tricalcium phosphate (β-TCP) phase content ratios before and after sintering at 1000°C for 1 hr as determined by XRD

Sample	Pre-sinter HA/ β-TCP ratio	Post-sinter HA/ β-TCP ratio
Biphasic		
HA/β-TCP	40/60	19/81
Biphasic		
HA//β-TCP	20/80	4/96

The post-sinter HA/β-TCP ratio was determined by the semi-quantitative XRD-based method via the X' Pert HighScore® analysis package.

Self-induction of bone formation in heterotopic sites, the *rectus abdominis* muscle

To determine intrinsic osteoinductivity imparted by surface geometry, monolithic discs of biphasic 19/81 and 4/96 HA/β-TCP fabricated with concavities on one planar surface only were implanted in the *rectus abdominis* muscle with the concavities either facing the dorsal or the ventral fasciae.

Both biphasic matrices induced the spontaneous induction of bone formation in the preformed concavities on day 90 and 365 after implantation in the *rectus abdominis* muscle (Figs. 3 and 4). Significant bone formation formed 365 days after implantation together with prominent resorption/dissolution of the biomimetic matrices coupled with progressive formation of bone replacing the implanted matrices (Fig. 4).

It was noteworthy that in both biphasic biomimetic matrices the planar surfaces without pre-cut concavities showed surface dissolution/resorption of the HA/β-TCP scaffolds by osteoclastic/macrophage cell-lines in the form of lacunae and concavities along the profile of the implanted linear planar surfaces (Figs. 3 and 4).

Resorption lacunae cut by macrophages and multinucleated giant cells initiated thus the induction of bone formation (Figs. 3 and 4). Bone matrix deposition extended and infiltrated within the biomimetic scaffolds under continuous resorption (Figs. 3H, K, L and 4K, L). There was a *continuum* of bone formation by induction together with a *continuum* of resorption/dissolution of the matrix resulting in lacunae and resorption pits which initiated the cascade of bone formation by induction eventually replacing the implanted biomatrices (Fig. 4G, K, L). Resorption/ dissolution of the biomatrix also initiated at the base of the pre-cut concavities with resorption lacunae invading the biomimetic constructs resulting in the induction of bone formation together with angiogenesis further resorbing the biomimetic matrices (Figs. 3K, L and 4H, J, K, L). Percentage of self-induced bone in different bioceramic constructs is presented in Table 1. Overall, no statistical differences could be found with respect of the orientation of the heterotopic discs as implanted in the *rectus abdominis* muscle (Table 1). Solid HA discs

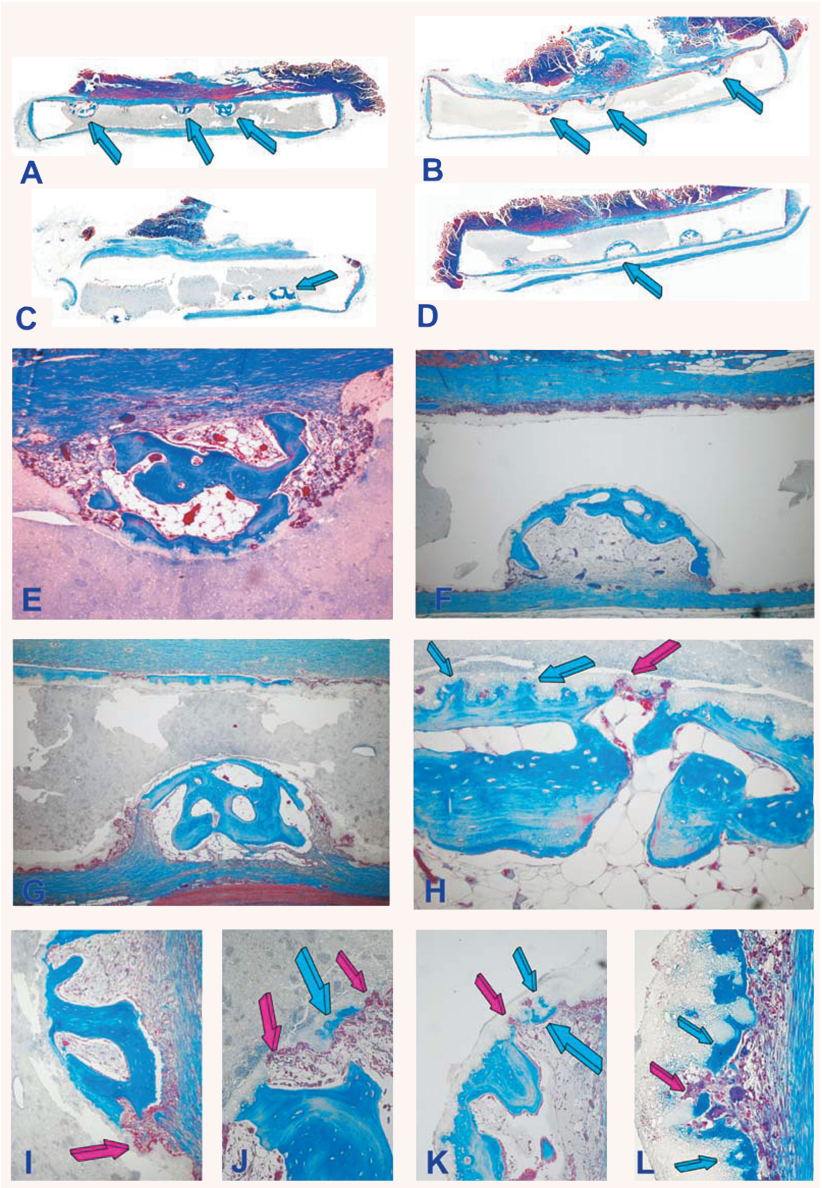

Fig. 3 Self-inducing geometric cues: the concavity, the shape of life and the induction of bone differentiation by *smart* biphasic hydroxyapatite/β-tricalcium phosphate biomimetic matrices 90 days after implantation in the *rectus abdominis* muscle of adult baboons *Papio ursinus* without the addition of exogenously applied osteogenic proteins; left panels (**A**, **C**, **E**, **G**, **I**, **J**) 19/81hydroxyapatite/β-tricalcium phosphate biomatrices; right panels (**B**, **D**, **F**, **H**, **K**, **L**) 4/96 hydroxyapatite/β-tricalcium phosphate biomatrices. (**A**, **C**) Low power views of 19/81 biphasic bioceramic discs showing substantial bone differentiation by induction within the concavities prepared along one planar surface only (arrows) either facing the *rectus abdominis* muscle (**A**, **B**) or the dorsal fascia of the muscle (**C**, **D**). (**E**, **G**) Induction of bone formation with marrow development and remodeling of the newly formed bone within the concavities. (**I**, **J**) Detail of the induction of bone by the substratum with macrophage/osteoclastic-like cells cutting resorption lacunae and pits (red arrows) with the shape of concavities promptly filled by newly formed bone by induction (blue arrows). (**F**, **H**, **K**, **L**) Induction of bone formation in concavities prepared in 4/96 hydroxyapatite/β-tricalcium phosphate bioceramics with more pronounced resorption/dissolution of the biomimetic matrices with induction of the newly formed bone within the biomimetic scaffolds (blue arrows in **H**). (**K**, **L**) Details of the morphological *continuum* of resorption/dissolution and *de novo* induction of bone at the resorptive front of the biomimetic matrix *via* cutting pits and lacunae (red arrows) promptly filled by newly formed bone (blue arrows). Decalcified sections cut at 4 μm stained with Goldner's trichrome. (**A**, **B**, **C**, **D**) original magnification ×3.7; (**E**) ×65; (**F**) ×45; (**I**, **J**, **K**, **L**) original magnification ×175.

showed lack of bone differentiation on day 90. Concavities cut in solid HA discs showed bone differentiation by induction on day 365 only (Table 1).

Morphology of calvarial regeneration and biphasic bioceramics incorporation

Because the initiation of bone formation is regulated by the geometry of the substratum, macroporous constructs of biphasic HA-β-TCP were sintered into biomimetic constructs with a sequence of repetitive concavities throughout the porous spaces (Fig. 2). Representative histological sections of calvarial defects implanted with biphasic HA/TCP 19/81 and 4/96 constructs harvested on day 90 and 365 are presented in Figures 5 and 6, respectively.

Porous spaces were filled by newly formed bone that initiated within the surface concavities of the macroporous spaces with direct bonding of bone to both biphasic bioceramics (Figs. 5 and 6). Dissolution and resorption of the HA/TCP scaffolds was evident on day 90 with newly forming bone replacing areas of resorbed matrix particularly evident in 4/96 HA/TCP biomatrices, which showed substantial bone formation by induction across the porous spaces as early as 90 days after calvarial implantation (Fig. 5B and C).

One year after implantation, both biphasic HA/TCP constructs but particularly the 4/96 constructs showed prominent resorption of the implanted biomimetic constructs replaced by newly formed

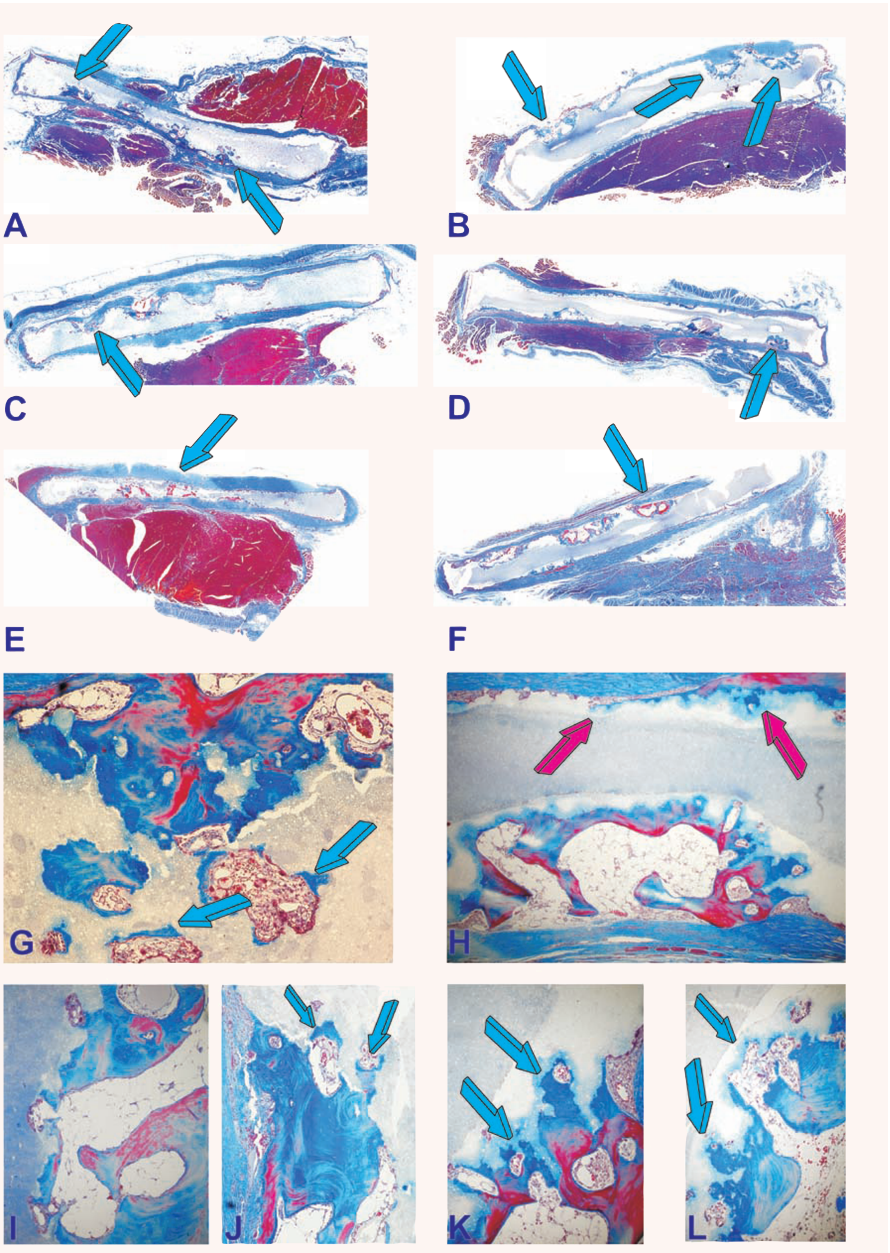

Fig. 4 Induction of bone formation (blue arrows) in concavities of post-sinter 19/81 (**A**, **C**, **E**) and 4/96 (**B**,**D**,**F**) hydroxyapatite/ β-tricalcium phosphate bioceramics implanted in the *rectus abdominis* muscle of adult baboons and harvested on day 365. (**G**, **I**, **J**) High power microphotographs detailing the induction of bone formation within newly cut lacunae of 19/81 biomatrices with replacement by newly deposited bone (blue arrows). (**H**, **K**, **L**) Morphological details of bone deposition by induction by 4/96 hydroxyapatite/β-tricalcium phosphate biomatrices showing bone deposition (blue arrows) in a *continuum* of morphological processes of resorption/dissolution and bone formation. The induction of bone is also visible along the planar surface of the implanted biomimetic construct (red arrows) with no pre-cut concavities along the planar surface (**H**). Original magnification: (**A**, **B**, **C**, **D**, **E**, **F**) ×3.7; (**G**, **H**) ×65 (**I**, **J**, **K**, **L**) ×175.

bone by induction ultimately greater than the profile of the normal calvaria (Fig. 6D). There was *restitutio ad integrum* of the calvarium, remodelling of the newly induced bone and resorption/dissolution of the guiding and inducing biomimetic matrix (Fig. 6D and F). Volume fraction compositions of calvarial specimens are presented in Table 3. On average, greater amounts of bone formed in 4/96 HA/TCP when compared to 19/81 biphasic constructs. The difference was statistically significant on day 365 only (Table 3). Greater resorption also characterized the 4/96 *versus* the 19/81 calvarial biphasic specimens (Table 3).

Discussion

This long-term study in adult primates demonstrates extensive induction of bone formation by biphasic biomimetic matrices implanted in both heterotopic *rectus abdominis* and orthotopic calvarial sites. More importantly, the initiation of bone formation by the biphasic biomimetic matrices progressed *via* a *continuum* of molecular and cellular events starting with osteoclastogenesis, the induction of resorption lacunae and concavities. This was then

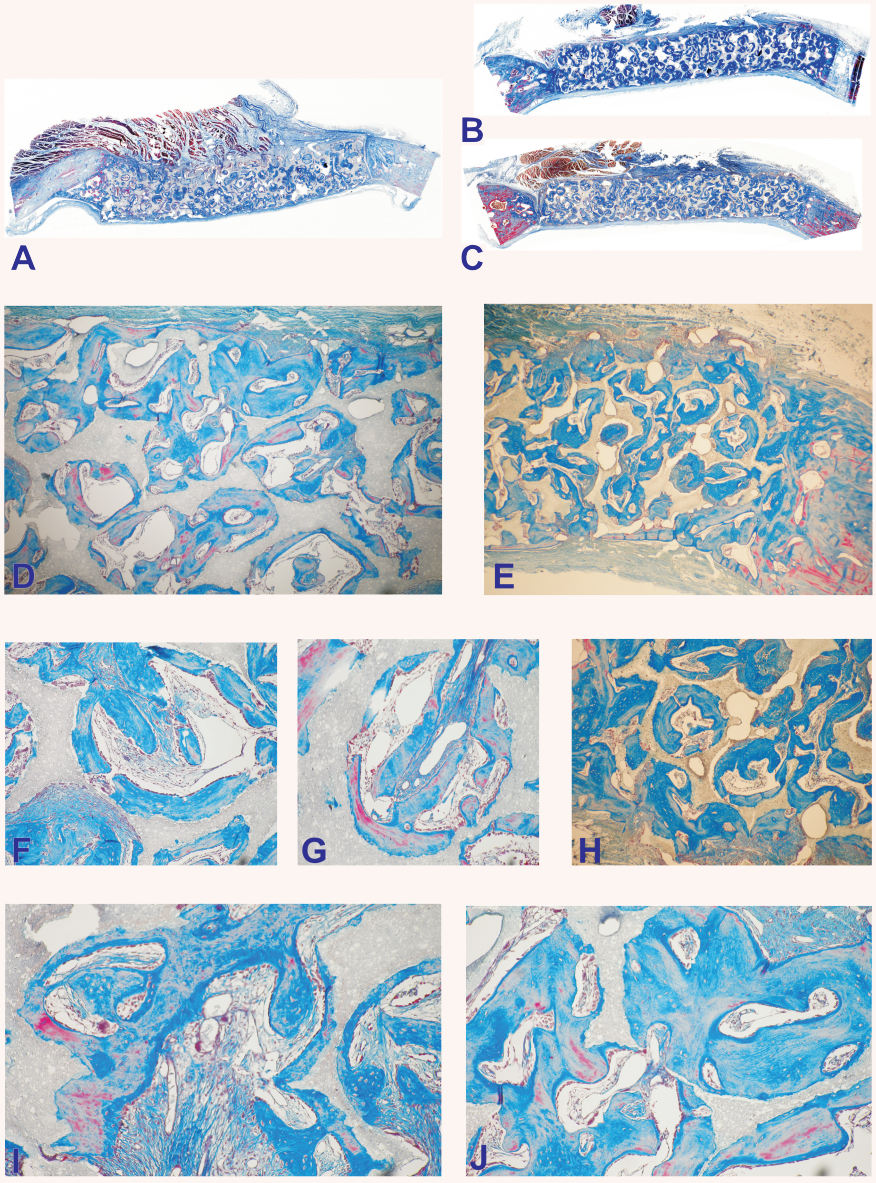

Fig. 5 Calvarial incorporation of 19/81 (**A**, **D**, **F**, **G**, **I**, **J**) and 4/96 (**B**, **C**, **E**, **H**) hydroxyapatite/β-tricalcium phosphate bioceramics harvested from the orthotopic calvarial sites 90 days after implantation. (**D**, **F**, **G**, **I**, **J**) microphotographic details of the induction of bone formation within the porous spaces of 19/81 hydroxyapatite/β-tricalcium phosphate bioceramics. (**B**, **C**) Substantial bone induction across specimens of 20/80 hydroxyapatite/β-tricalcium phosphate bioceramics with bone differentiation by induction (**E**, **H**) across the porous spaces of the substratum. Original magnification: (**A**, **B**, **C**) ×2.7 (**B**) ×125; (**G**, **H**) ×65; (**I**, **J**, **K**, **L**) ×175.

followed by the induction of bone formation within the newly formed resorptive pits, lacunae and concavities. The concavities are initiators of bone formation by induction when implanted in the *rectus abdominis* muscle of *Papio ursinus* [2, 41]. Resorption thus initiated the induction of bone formation in a *continuum* of molecular and morphological processes that resulted in significant amounts of bone formation replacing the implanted biomimetic matrices. The significant induction of bone formation without the addition of osteogenic proteins additionally shows a novel delivery system for the osteogenic proteins of the TGF-β superfamily [20] for the rapid induction of clinically relevant bone formation in human patients.

Biphasic calcium phosphate bioceramics, formed by mixing non-resorbable hydroxyapatite (HA: $Ca_{10}(PO_4)_6(OH)_2$) with resorbable β-tricalcium phosphate (β-TCP: β-$Ca_3(PO_4)_2$) [23, 24], are highly suitable materials for synthetic bone substitute applications because the HA provides a permanent scaffold for the formation of new bone *via* both osteoconduction and osteoinduction. The resorption of the β-TCP over-saturates the local environment with Ca^{2+} and PO_4^{3-} ions and accelerates the induction of bone

Table 3 Volume fraction (%) of tissue components in porous biphasic hydroxyapatite (HA)/ β tricalcium phosphate (β-TCP) implanted in 16 calvarial defects of 4 adult baboons and harvested 90 and 365 days after implantation

Time	Biomimetic Matrices HA/β-TCP	Bone	Matrix	FVA
90	19/81 HA/β-TCP	37.7 ± 3.9	28.5 ± 1.3	33.8 ± 0.8
	4/96 HA/β-TCP	39.7 ±3.5	21.6 ±1.3	38.7 ±2.5
365	19/81 HA/β-TCP	53.7 ± 3.4	26.6 ± 2.4	19.7 ± 2.7
	4/96 HA/β-TCP	73.7 ± 3.5*	6.9 ± 3.0*	19.4 ± 2.3

Volume fractions (%) of tissue components in orthotopic calvarial specimens were calculated with a calibrated Zeiss Integration Platte II with 100 lattice points superimposed over five sources selected for histomorphometry in each section as described in 'Materials and methods'. Values are given as means ± SEM of 4 specimens per treatment modality representing two animals per observation period. * $P < 0.05$ *versus* 19/81 on day 90 and 365.

formation within the porous spaces of the biphasic constructs [34]. The rate and extent of biphasic calcium phosphate bioceramics resorption *in vivo*, at least in rat, rabbit and canine models, is predominantly determined by the HA:β-TCP phase content ratio; higher β-TCP contents allow faster and more pronounced resorption [23, 35, 36]. The resorption rate should ideally be matched to the rate of new bone formation, and thus the HA/β-TCP phase content ratio is a critical parameter to control during synthesis. Biphasic bioceramics typically have a β-TCP content of 40wt% (balance HA), although Livingstone Arinzeh *et al.* [37] have recently reported that biphasic bioceramics with 80wt% β-TCP content gave the highest rate of human mesenchymal stem cell-induced osteoinduction in a heterotopic mouse model [37].

After millions of years of evolution, Nature has had the capacity to nucleate and evolve highly sophisticated tissues and organs [2, 15]; we have also learned that Nature relies on common yet limited mechanisms tailored to provide the emergence of specialized tissue and organs [1, 2, 13, 20]. Indeed, to initiate the induction of bone formation and thus to ultimately erect the skeleton, Nature has had a powerful lesson to teach [1, 2, 38–40]. The distilled summary of millions of years of evolution is surprisingly simple: first, tissue induction in post-natal life recapitulates events that occur in the normal course of embryonic development, and second, that both embryonic development and tissue induction and morphogenesis in post-natal life are equally regulated by selected few and highly conserved families of morphogens [1, 2, 13, 20]. The induction of bone formation requires three key components [1]: an osteoinductive soluble molecular signal, an insoluble signal or substratum and responding host's cells. Soluble and insoluble signals need to be reconstituted or recombined to trigger the bone induction cascade [1, 2, 14, 15, 38, 39]. A most fascinating and novel strategy to initiate the induction of bone formation is to construct biomimetic bioactive biomaterial matrices that *per se* initiate the morphogenesis of bone even when implanted in heterotopic extraskeletal sites and without exogenously applied osteogenic soluble molecular signals of the TGF-β superfamily [2, 14–20, 38–41].

Systematic studies in the non-human primate *Papio ursinus* have shown that the driving force of the intrinsic induction of bone formation by bioactive biomimetic matrices is the shape of the implanted scaffold [2, 19, 38–41]; the language of shape is the language of geometry: the language of geometry is the language of a sequence of repetitive concavities that biomimetizes the remodelling cycle of the primate osteonic bone [2, 14, 38, 39]. It was noteworthy that this study has clearly shown that lacunae and concavities cut by osteoclastogenesis within the sintered HA/β-TCP matrices are driving the morphogenesis of bone, further resorption and dissolution ultimately replacing the implanted biomimetic matrices by newly formed bone by induction and without the exogenous application of the soluble molecular signals of the TGF-β superfamily [20]. The process is a *continuum* of sequential phases of resorption/dissolution and induction of bone formation; high power morphological evaluation of newly formed concavities by osteoclast/macrophage-like cells show the intimate relationship between osteoclasts/macrophages and osteoblastic cells in a *continuum* of secretory processes ultimately leading to the effacement of the implanted matrices and its replacement by newly formed bone.

Recently, the lexicon of regenerative medicine and tissue engineering has been enriched by the introduction of the term biomimetism, meaning of the creative imitation of various specific biological systems [38–46]. Biomimetism is gaining inspiration from Nature to tailor novel biomaterial matrices inspired by biological structures that Nature has carved [38–46]. The described biphasic HA/ β-TCP biomatrices biomimetize the remodelling cycle of the bone unit or osteosome [47] *via* a *continuum* of resorption and bone deposition initiated by the concavities in the form of resorption lacunae and pits cut by osteoclastogenesis and used for the deposition of bone by induction. Using a post-sinter 4/96 HA/β-TCP ratio, this study shows complete calvarial bone

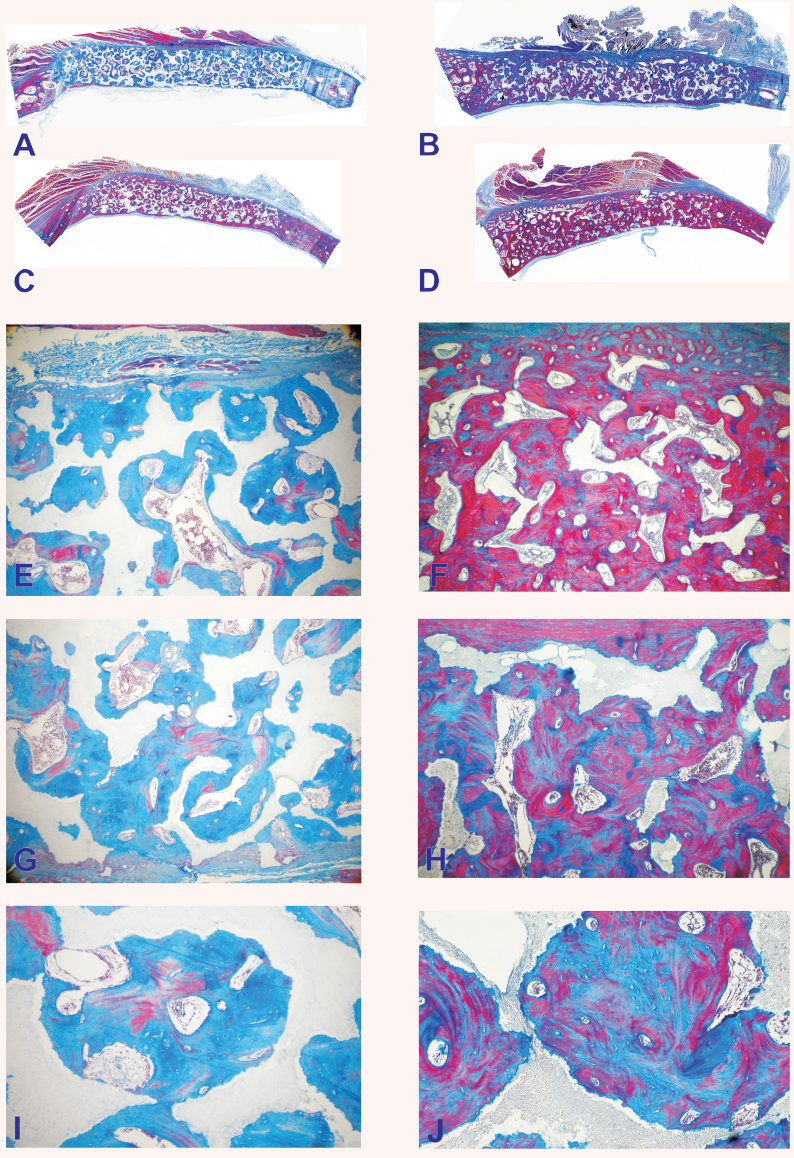

Fig. 6 Calvarial incorporation of post-sinter 19/81 (**A**, **C**, **E**, **G**, **I**) and 4/96 (**B**, **D**, **F**, **H**, **J**) hydroxyapatite/β-tricalcium phosphate bioceramics harvested from the orthotopic calvarial sites 365 days after implantation. (**A**, **C**) Low power view of substantial bone induction across specimens of 19/81 hydroxyapatite/β-tricalcium phosphate bioceramics. (**E**, **G**, **I**) Morphological details of bone induction across the porous spaces and attachment of the newly formed bone to the hydroxyapatite substratum. (**B**, **D**) Bone formation by induction across specimens of 4/96 hydroxyapatite/β-tricalcium phosphate bioceramics showing extensive induction of bone formation with replacement of the implanted biomatrix and with *restitutio ad integrum* of the implanted calvarial defect. (**F**, **H**, **J**) Microphotographic details showing the induction of bone across the porous spaces of the biomimetic matrix with solid block of newly formed bone replacing the implanted biomimetic scaffold. Original magnification: (**A**, **B**, **C**, **D**) ×2.7; (**E**, **F**, **G**, **H**) ×35; (**I**, **J**) ×75.

regeneration *with restitutio ad integrum* of the defect 1 year after operation.

In a canine model, Kondo *et al.* [48] showed osteoinduction by highly purified β-tricalcium phosphate in heterotopic intramuscular sites [48]. Six months after implantation of the β-TCP constructs, the implanted samples significantly resorbed as evaluated morphometrically 168 days after heterotopic implantation [48]. The appearance of a large number of active osteoclasts preceded the induction of bone formation probably by cutting resorption lacunae and/or pits initiating thus the induction of bone formation.

In comprehensive experiments by Yuan *et al.* [49] investigating the cross-species induction of heterotopic bone formation by biphasic calcium phosphate and hydroxyapatite bioceramics, it was found that biphasic calcium phosphates sintered at a relatively low temperature have a higher osteoinductive potential than hydroxyapatites sintered at higher temperatures [49]. In other studies, the

same authors reported the long-term material-dependent bone induction by calcium phosphate bioceramics in a canine model reporting that the induced bone remained stable through bone remodelling up to 2.5 years after heterotopic implantation [50].

Remarkably, the ligature of the renal artery induces the induction of bone in the kidney' parenchyma [51]. This was followed by the fascinating observation of uroepithelial osteogenesis [52]. CB Huggins defined the phenomenon that occurred after heterotopic transplantation of bladder mucosa into the *rectus abdominis* and fascia of the *rectus abdominis* muscle into the dome of the bladder [52]. Of great interest since described in rats, Selye *et al.* [53] reported the induction of bone, cartilage and haematopoietic tissue after subcutaneous implantation of tissue diaphragms 53]. The heterotopic induction of bone formation was later reported in the subcutaneous space and skin of a porcine model after implantation of polyhydroxyethyl-methacrylate sponges [54]. Since the introduction of biphasic bioceramics in pre-clinical contexts in a variety of animal models including goats [55] and non-human primates [19], biphasic HA/β-TCP constructs of 20/80 HA to β-TCP and higher HA content have been implanted in human patients with varying degrees of success [56–59].

To summarize, the reconstitution of a soluble osteogenic molecular signal with an insoluble signal or substratum that delivers the biological activity of the osteogenic soluble molecular signals of the TGF-β superfamily has been and still is the molecular paradigm of regenerative medicine, tissue engineering and morphogenesis. We have presented a modified paradigm in which the very insoluble signal or substratum resorbs *via* a downstream of molecular and cellular cascades that sculpt resorption pits and lacunae in the geometric form of concavities within the implanted tricalcium phosphate/ hydroxyapatite biomatrices. The concavities as sculpted within the implanted biomimetic matrices initiate bone differentiation by induction. The operational molecular and cellular resorption and dissolution of the implanted matrices sculpting lacunae and pits in the form of concavities are the biological *continuum* for the induction of bone formation. There is thus a *continuum* between the soluble and solid states of the newly formed bone as in the skeleton [47] in which the *continuum* is regulated by signals in solution interacting with the insoluble extracellular matrix [47]. The implanted biomimetic matrices or insoluble signals regulate the expression of the soluble osteogenic molecular signals of the TGF-β superfamily [20] initiating the cascade of bone differentiation by induction [2, 20].

We have previously asked [2, 19] if tissue engineers and skeletal reconstructionists alike could design biomimetic matrices capable *per se* of expressing selected mRNA species of the TGF-β superfamily embedded within the specific geometry of the biomimetic matrices, *i.e.* a bioactive matrix that in its own right expresses the molecular signals endowed with the striking prerogative of initiating bone differentiation by induction [2, 19]. We show now that the spontaneous induction of bone formation is a recapitulation of embryonic bone development that biomimetizes and recapitulates the bone remodelling cycle of primate bone *via* the sculpting of resorption lacunae which set into motion the ripple-like cascade of bone deposition by induction ultimately replacing the implanted biomimetic matrices.

If the concept of regenerative medicine and tissue engineering is 'the persuasion of the body to heal itself through the delivery to the appropriate site of cells, biomolecules and/or supporting structures' [60], we must now consider the fundamental role of the substratum, or insoluble signal, that deliver or induce, as shown here, the soluble osteogenic molecular signals and that control osteogenesis in pre-clinical and clinical contexts [2, 20].

Tissue engineers, biomaterials scientists and molecular biologists alike must always however remember that remarkably, the geometric configuration of the substratum can inhibit and overrule the osteogenic activity of the osteogenic soluble molecular signals of the TGF-β superfamily [20] in rodents [61] as well as non-human primates [62]. There is no bone formation by induction without the osteogenic proteins of the TGF-β superfamily [20, 39]; recombination is however required to deliver the osteogenic activity of the soluble osteogenic molecular signals [1, 2, 20]; the architectural geometric configuration of the implanted biomatrices ultimately controls the significant induction of bone formation in pre-clinical and clinical contexts.

Acknowledgements

Supported by the South African Medical Research Council, the University of the Witwatersrand, Johannesburg, the National Research Foundation, the Council for Scientific and Industrial Research, and by *ad hoc* grants of the Bone Research Unit. We thank the Central Animal Services of the University for the help with primate experimentation.

References

1. **Reddi AH.** Morphogenesis and tissue engineering of bone and cartilage: Inductive signals, stem cells, and biomimetic biomaterials. *Tissue Eng.* 2000; 6: 351–9.
2. **Ripamonti U.** Soluble osteogenic molecular signals and the induction of bone formation. *Biomaterials.* 2006; 27: 807–22.
3. **Gautschi OP, Frey SP, Zellweger R.** Bone morphogenetic proteins in clinical applications. *ANZ J Surg.* 2007; 77: 626–31.
4. **Garrison KR, Donnell S, Ryder J, Shemilt I, Mugford M, Harvey I, Song F.** Clinical effectiveness and cost-effectiveness of bone morphogenetic proteins in the non-healing of fractures and spinal fusion: a systematic review. *Health Technol Assess.* 2007; 11: 1–150.
5. **Einhorn TA.** Clinical applications of recombinant human BMPs: early experience and future development. *J Bone Joint Surg Am.* 2003; 85-A: 82–8.
6. **Mussano F, Ciccone G, Ceccarelli D, Baldi I, Bassi F.** Bone morphogenetic

proteins and bone defects. A systematic review. *Spine*. 2007; 32: 824–30.
7. **Termaat MF, Den Boer FC, Bakker FC, Patka P, Haarman, HJ.** Bone morphogenetic proteins. Development and clinical efficacy in the treatment of fractures and bone defects. *J Bone Joint Surg Am*. 2005; 87: 1367–78.
8. **Groeneveld EHJ, Burger EH.** Bone morphogenetic proteins in human bone regeneration. *Eur J Endocrinol*. 2000; 142: 9–21.
9. **Boyne PJ, Lilly LC, Marx RE, Moy PK, Nevins M, Spagnoli DB, Gilbert Triplett R.** De novo bone induction by recombinant human bone morphogenetic protein – 2 (rhBMP-2) in maxillary sinus floor augmentation. *J Oral Maxillofac Surg*. 2005; 63: 1693–707.
10. **Friedlaender GE, Perry CR, Cole JD, Cook SD, Cierny G, Muschler GF, Zych GA, Calhoun JH, LaForte Aj, Yin S.** Osteogenic protein-1 (bone morphogenetic protein-7) in the treatment of tibial nonunions. *J Bone Joint Surg Am.* 2001; 83A: S151–8.
11. **Govender S, Csimma C, Genant HK, Valentin-Opran A, Amit Y, Arbel R, Aro H, Atar D, Bishay M, Börner MG, Chiron P, Choong P, Cinats J, Courtenay B, Feibel R, Geulette B, Gravel C, Hass N, Raschke M, Hammacher E, van der Velde D, Hardy P, Holt M, Josten C, Ketterl RL, Lindeque B, Lob G, Mathevon H, McCoy G, Marsh D, Miller R, Munting E, Oevre S, Nordsletten L, Patel A, Pohl A, Rennie W, Reynders P, Rommens PM, Rondia J, Rossouw WC, Danell PJ, Ruff S, Rüter A, Santavirta S, Schildhauer TA, Gekle C, Schnettler R, Segal D, Seiler H, Snowdowne RB, Stapert J, Taglang G, Verdonk R, Vogels L, Weckbach A, Wentzensen A, Wisniewski T.** Recombinant human bone morphogenetic protein-2 for treatment of open tibial fractures: a prospective, controlled, randomized study of four hundred and fifty patients. *J Bone Joint Surg Am.* 2002; 84A: 2123–34.
12. **Reddi AH.** Bone and cartilage differentiation by bone morphogenetic proteins. *Curr Opin Genet Dev*. 1994; 4: 737–44.
13. **Reddi AH**. Role of morphogenetic proteins in skeletal tissue engineering and regeneration. *Nature Biotechnol*. 1998; 16: 247–52.
14. **Ripamonti U, Ramoshebi LN, Matsaba T, Tasker J, Crooks J, Teare J.** Bone induction by BMPs/OPs and related family members in primates. The critical role of delivery systems. *J Bone Joint Surg*. 2001; 83: 116–27.
15. **Ripamonti U, Ramoshebi LN, Patton J, Matsaba T, Teare J, Renton L.** Soluble signals and insoluble substrata: novel molecular cues instructing the induction of bone. In: Massaro EJ, Rogers JM, editors. The skeleton. Totowa, NJ: *Humana Press;* 2004. pp. 217–27.
16. **Ripamonti U, Ramoshebi LN, Patton J, Teare J, Matsaba T, Renton L.** Sculpting the architecture of mineralized tissue: tissue engineering of bone from soluble signals to smart biomimetic matrices. In: Muller RH, Kayser O, editors. *Pharmaceutical biotechnology. Weinheim: Wiley-VCH*; 2004. pp. 281–97.
17. **Ripamonti U, Ma S-S, Reddi AH.** Induction of bone in composite of osteogenin and porous hydroxyapatite in baboons. *Plast Recontsr Surg*. 1992; 89: 731–39.
18. **Ripamonti U, Ma S-S, van den Heever B, Reddi AH.** Osteogenin, a bone morphogenetic protein, adsorbed on porous hydroxyapatite substrata, induces rapid bone differentiation in calvarial defects of adult primates. *Plast Reconstr Surg*. 1992; 90: 382–93.
19. **Ripamonti U, Richter PW, Thomas ME.** Self-inducing shape memory geometric cues embedded within *smart* hydroxyapatite-based biomimetic matrices. *Plast Reconstr Surg*. 2007; 120: 1–12.
20. **Ripamonti U.** Osteogenic proteins of the TGF-β superfamily. In: Henry HL, Norman AW, editors. Encyclopedia of hormones. San Diego, CA: *Austin Academic Press*; 2004. pp. 80–6.
21. **LeGeros RZ, LeGeros JP.** Dense hydroxyapatie. In: Hench LL, Wilson J, editors. An introduction to bioceramics. Singapore: *World Scientific Publishing*; 1993. pp. 139–80.
22. **Ramachandra Rao R, Rai R, Roopa HN, Kannan TS.** Solid state synthesis and thermal stability of HAP and HAP-β-TCP composite ceramic powders. *J Mater Sci: Mater Med*. 1997; 8: 511–18.
23. **Fazan F, Shahida KBN.** Fabrication of synthetic apatites by solid state reactions. *Med J Malaysia.* 2004; 59: 69–70.
24. **Daculsi G, LeGeros RZ, Nery E, Lynch K, Kerebel B.** Transformation of biphasic calcium phosphate ceramics in vivo: ultrastructural and physicochemical characterization. *J Biomed Mater Res.* 1989; 23: 883–94.
25. **Nilen RWN, Richter PW.** The thermal stability of hydroxyapatite in biphasic calcium phosphate ceremics. *J Mat Sci: Mater Med*. Epub 2007; 19: 1693–702.
26. **Chung FH.** Quantitative interpretation of X-ray diffraction patterns, I. Matrix flushing method of quantitative multicomponent analysis. *J Appl Cryst*. 1974; 7: 513–19.
27. **Ripamonti U.** The morphogenesis of bone in replicas of porous hydroxyapatite obtained from conversion of calcium carbonate exoskeletons of coral. *J Bone Joint Surg*. 1991; 73-A: 692–703.
28. **Public Service Department.** National code for animal use in research, education, diagnosis and testing of drugs and related substances in South Africa. *Public Service Department, Pretoria, South Africa;* 1990.
29. **Parfitt AM.** Stereologic basis of bone histomorphometry; theory of quantitative microscopy and reconstruction of the third dimension. In: Recker HR, editor. Bone hystomorphometry: techniques and interpretation. *Boca Raton: CRC Press*; 1983. pp. 53–87.
30. **Landi E, Ampieri A, Celotti G, Sprio S.** Densification behaviour and mechanisms of synthetic hydroxyapatites. *J Eur Ceramic Soc.* 2000; 20: 2377–87.
31. **Raynaud S, Champion E, Bernache-Assollant D, Thomas P.** Calcium phosphate apatites with variable Ca/P atomic ratio I. Synthesis, characterisation and thermal stability of powders. *Biomaterials*. 2002; 23: 1065–72.
32. **Lin F-H, Chun-Jen L, Ko-Shao C, Jui-Sheng S.** Thermal reconstruction behaviour of the quenched hydroxyapatite powder during reheating in air. *Mat Sci Eng*. 2000; 13: 97–104.
33. **Klein CPAT, Wolke JGC, de Groot K.** Stability of calcium phosphate ceramics and plasma sprayed coating. In: Hench LL, Wilson J, editors. An introduction to bioceramics. Singapore: *World Scientific Publishing;* 1993. pp. 199–221.
34. **Vallet-Regi M, Gonzalez-Calbet JM.** Calcium phosphates as substitution of bone tissues. *Prog Solid State Chem*. 2004; 32: 1–31.
35. **Yamada S, Heymann D, Bouler JM, Daculsi G.** Osteoclastic resorption of calcium phosphate ceramics with different hydroxyapatite/β-tricalcium phosphate ratios. *Biomaterials*. 1997; 18: 1037–41.
36. **Daculsi G.** Biphasic calcium phosphate concept applied to artificial bone implant coating and injectable bone substitute. *Biomaterials.* 1998; 19: 1473–8.
37. **Livingstone Arinzeh T, Tran T, Mcalary J, Daculsi G.** A comparative study of biphasic

calcium phosphate ceramics for human mesenchymal stem-cell-induced bone formation. *Biomaterials*. 2005; 26: 3631–8.
38. **Ripamonti U.** Soluble, insoluble and geometric signals sculpt the architecture of mineralized bone. *J Cell Mol Med*. 2004; 8: 169–80.
39. **Ripamonti U.** Biomimetism, biomimetic matrices, and the induction of bone formation. *J Cell Mol Med*. 2007; submitted.
40. **Ripamonti U, Duneas N.** Tissue engineering of bone by osteoinductive biomaterials. *MRS Bulletin*. 1996; 21: 36–9.
41. **Ripamonti U, Crooks J, Kirkbride AN.** Sintered porous hydroxyapatites with intrinsic osteoinductivity activity: geometric induction of bone formation. *S Afr J Sci*. 1999; 95: 335–43.
42. **Sanchez C, Arribart H, Giraud Guille MMG.** Biomimetism and bioinspiration as tools for the design of innovative materials and systems. *Nature Mat*. 2005; 4: 277–88.
43. **Fratzl P.** Biomimetic materials research: what can we really learn from nature's structural materials? *J R Soc Interface*. 2007; 4: 637–42.
44. **Ingber DE, Mow VC, Butler D, Niklason L, Huard J, Mao J, Yannas I, Kaplan D, Vunjak-Novakovic G.** Tissue engineering and developmental biology: going biomimetic. *Tissue* Eng. 2006; 12: 3265–83.
45. **Sarikaya M.** Biomimetics: materials fabrication through biology. *Proc Natl Acad Sci USA*. 1999; 96: 14183–85.
46. **Tamerler C, Sarikaya M.** Molecular biomimetics: utilizing nature's molecular ways in practical engineering. *Acta Biomaterialia*. 2007; 3: 289–99.
47. **Reddi AH.** Bone morphogenesis and modeling: soluble signals sculpt osteosomes in the solid state. *Cell* 1997; 89: 159–61.
48. **Kondo N, Ogose A, Tokunaga K, Umezu H, Arai K, Kudo N, Hoshino M, Inoue H, Irie H, Kuroda K, Mera H, Endo N.** Osteoinduction with highly purified β-tricalcium phosphate in dog dorsal muscles and the proliferation of osteoclasts before heterotopic bone formation. *Biomaterials*. 2006; 27: 4419–27.
49. **Yuan H, Van Blitterswijk A, De Groot K, De Bruijn JD.** Cross-species comparison of ectopic bone formation in biphasic calcium phosphate (BCP) and hydroxyapatite (HA) scaffolds. *Tissue Eng*. 2006; 12: 1607–15.
50. **Yuan H, Yang Z, De Bruijn JD, De Groot K, Zhang X.** Material-dependent bone induction by calcium phosphate ceramics: q 2.5-year study in dog. *Biomaterials*. 2001; 22: 2617–23.
51. **Sacerdotti C, Frattin G.** Sulla produzione eteroplastica dell'osso. *R Accad Med Torino*. 1901; 27: 825–36.
52. **Huggins CB.** The formation of bone under the influence of epithelium of the urinary tract. *Arch Surg*. 1931; 22: 377–408.
53. **Selye H, Lemire Y, Bajusz E.** Induction of bone, cartilage and hemopoietic tissue by subcutaneously implanted tissue diaphragms. *Wilhelm Roux' Arch Entwickl-Mech Org*. 1960; 151: 572–85.
54. **Winter GD, Simpson BJ.** Heterotopic bone formed in a synthetic sponge in the skin of young pigs. *Nature*. 1969; 223: 88–90.
55. **Fellah BH, Gauthier O, Weiss P, Chappard D, Layrolle P.** Osteogenicity of biphasic calcium phosphate ceramics and bone autografts in a goat model. *Biomaterials*. 2008; 29: 1177–88.
56. **Delécrin J, Takahashi S, Gouin F, Passuti N.** A synthetic porous ceramic as a bone graft substitute in the surgical management of scoliosis: a prospective, randomized study. *Spine*. 2000: 25: 563–9.
57. **Cho DY, Lee WY, Sheu PC, Chen CC**. Cage containing a biphasic calcium phosphate ceramic (Triosite) for the treatment of cervical *spondylosis*. *Surg Neurol*. 2005; 63: 497–503.
58. **Xie Y, Chopin D, Morin C, Hardouin P, Zhu Z, Tang J, Lu J.** Evaluation of the osteogenesis and biodegradation of porous biphasic ceramic in the human spine. *Biomaterials*. 2006; 27: 2761–7.
59. **Malard O, Espitalier F, Bordure P, Daculsi G, Weiss P, Corre P.** Biomaterials for tissue reconstruction and bone substitution of the ear, nose and throat. *Expert Rev Med Devices*. 2007; 4: 729–39.
60. **Williams DF.** Tissue engineering: the multidisciplinary epitome of hope and despair. In: Paton R, McNamare L, editors. Studies in multidisciplinarity. Amsterdam: *Elsevier* BV; 2006. pp. 483–524.
61. **Ripamonti U, Ma S, Reddi AH.** The critical role of geometry of porous of porous hydroxyapatite delivery systems in induction of bone by osteogenin, a bone morphogenetic protein. *Matrix*. 1992; 12: 202–12.
62. **van Eeden SP, Ripamonti U.** Bone differentiation in porous hydroxyapatite in baboons is regulated by the geometry of the substratum substratum: implications for reconstructive craniofacial surgery. *Plast Reconstr Surg*. 1994; 93: 959–66.